Proceedings of the 5th International Conference on Vibration Engineering, Nanjing, China, September 18-20, 2002

BEARING DYNAMIC CHARACTERISTICS OF THE VENTRASSIST ROTARY BLOOD PUMP

M. Chung[1], N. Zhang[1], G.D. Tansley[2] and J.C. Woodard[2]

[1] Faculty of Engineering, University of Technology, Sydney, 1 Broadway NSW 2007, Australia
[2] VentrAssist P/L, 126 Greville Street Chatswood NSW 2067, Australia

Abstract The VentrAssist implantable rotary blood pump, intended for long term ventricular assist, is under development and is currently being tested for its rotor-dynamic stability. A shaftless impeller, which also acts as the rotor of the brushless DC motor, is passively suspended in the pump cavity by hydrodynamic forces.

The paper presents experimental investigation of the displacement of the impeller within the cavity, which will play an integral role in obtaining approval for clinical trials.

Displacement of the impeller is measured using Hall effect sensors located at different positions on the pump under different pump-operating conditions. Voltage output from the sensors are converted into impeller movement in five degrees of freedom (x, y, z, θ_x and θ_y). The sixth degree of freedom (θ_z), the rotation about the impeller axis, is determined by the commutation performed by the motor controller.

To determine experimentally the undamped dynamic characteristic of the hydrodynamic bearing, future measurements of bearing forces combined with the results of impeller displacement presented in this paper will allow for the calculation of stiffness coefficients for the hydrodynamic bearing.

Keywords: rotor dynamics, hydrodynamic bearing, rotary blood pump

1. Introduction

The VentrAssist implantable rotary blood pump is based on a centrifugal design and is intended for long term ventricular assist. It is currently under development and being tested for its rotor-dynamic stability. It is a novel device consisting of only one moving part – a shaftless impeller. The impeller blades are imbedded with permanent magnets to enable it to act as a rotor for the pump's brushless DC motor. Suspension of the impeller within the pump cavity is performed passively and is achieved through the use of hydrodynamic forces on both the bottom bearing pad and the conical surface. Hydrodynamic suspension has been investigated by other parties[1,2], while others incorporate hydrodynamic bearings working in synergy with magnetic bearings for suspension[3]. Active suspension systems are currently being utilised by other rotary blood pumps[4,5,6]; however, these incorporate more complex and larger monitoring and electrical systems. With the VentrAssist pump, monitoring sensors are eliminated due to the use of hydrodynamic bearings for passive suspension, thus requiring less complicated electronics. This results in a smaller, more efficient pump.

Due to the absence of monitoring sensors in the VentrAssist pump, the movement of the impeller within the pump cavity is unknown. Therefore, in this paper, the impeller displacement during operating conditions was evaluated experimentally through displacement measurements using hall effect sensors.

Previous impeller displacement measurements, using eddy current proximity sensors and laser proximity sensors, had been investigated by the authors. Although results were in agreement with centrifugal pump design theory, the accuracy of these results were debatable. The eddy current proximity sensors operate ideally when the target surface area (bottom surface of the blade) is at least three times the size of the sensor head. In the case of the experiment, the sensor head was almost identical in size to the target surface area, thus producing results that were not exact.

A more accurate means of measuring the impeller displacement has been developed here through the use of hall effect sensors. Hall effect sensors measure magnetic field strengths, and since the impeller is imbedded with permanent magnets, these sensors were ideal for impeller measurements.

2. Background

2.1 Hydrodynamic bearing

The suspension of the impeller within the pump cavity is due to the hydrodynamic forces from the bearing[7,8], which are a result of the small clearances between the outer surfaces of the impeller and the pump cavity. These clearances range from approximately 50μm to 200μm in nominal size. The impeller blade surfaces incorporate a wedge design where the leading edge clearance is larger than the trailing edge clearance (Fig. 1).

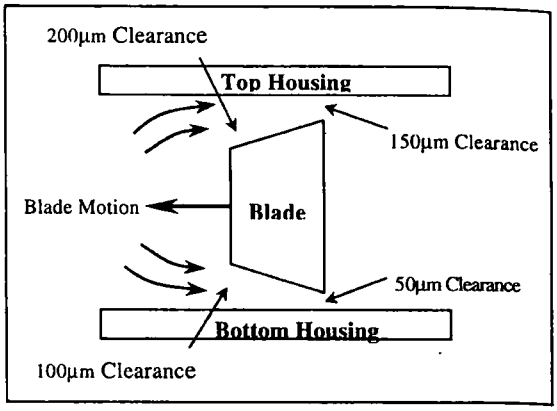

Fig. 1 Wedge design of the hydrodynamic bearing

By using this wedge design, basic 2-dimensional hydrodynamic lubrication theory[9] can be applied to determine the pressure force:

$$F = 0.15888 \frac{\mu V l^2 \omega}{h^2} \quad (1)$$

Where bearing pressure force (F) is a function of viscosity (μ), speed (V), length (l) and clearance (h). Also, velocity and length are a function of radius (r) of the impeller.

As the bearing clearance decreases, say towards the bottom housing, the pressure force increases (Fig. 2) until the blade touches causing an infinite pressure force acting on the blade.

With the wedge design incorporated into the VentrAssist impeller at both the top and bottom surfaces, pressure forces will be experienced at both these locations. An equilibrium position will be achieved when both top and bottom forces are of equal magnitude and opposite direction.

2.2 Hall effect sensors

The concept behind the Hall effect is simply the detection of a magnetic field. When the sensor is passed through a magnetic field (B) which is perpendicular to both the current (I) and output connections, a Lorentz force is exerted on the current. This force disturbs the current distribution, resulting in a potential difference (Hall voltage - V_H) across the output.

This potential difference is proportional to the interaction of the magnetic field and the current as shown in equation 2.

$$V_H \propto I \times B \quad (2)$$

The Hall effect sensors used for the experiment are of the analog type, where a voltage output proportional to the supply voltage is given. Calibration of these sensors was first carried out for displacement measurements.

3. Materials and Method

A laboratory version of a VentrAssist C-D pump housing and a 2.8 series impeller was used for the experiment. The pump housing and impeller was made of titanium aluminium vanadium (Ti-6Al-4V), a biocompatible alloy. Generally the pump will operate using six electromagnetic coils, three on the body (cone) and three on the cover (base). However, due to the Hall effect sensors being sensitive to magnetic fields produced by the actuation of the coils, the coils on the cover were removed to accommodate the sensors. The electrical design of the pump allows it to continue operating normally with only the one set of coils remaining on the body. Hydrodynamic stability of the impeller is not jeopardised.

The magnets of the impeller are configured so that like poles are on opposite blades (Fig. 2). The magnetic flux (kilo-Maxwell-turns) of each blade was measured using a flux meter (Model 2130 Fluxmeter – Magnetic Instrumentation Inc., USA). The measured flux was converted to magnetic field strength using equation 3.

$$B = \frac{\Phi}{A \times t \times 10^8} \quad (3)$$

Where B is the magnetic field strength measured in Tesla (T), Φ is the magnetic flux measured from the meter, A is the cross sectional area of the measuring coil and t is the number of turns in the coil.

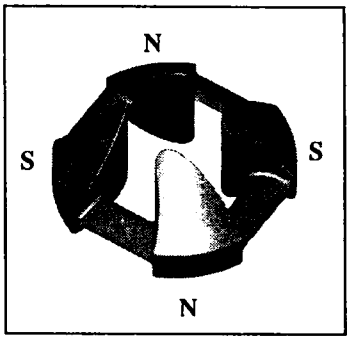

Fig. 2 Pole configuration for 2.8 impeller

Six Hall effect sensors (Honeywell SS495A1) were distributed on the x and y plane of the cover, with four on the bottom of the cover and the remaining two on the side of the cover (Fig. 3). The sensors located on the bottom were used to measure the axial (z) and angular (θx and θy) displacement of the impeller, at 90° degree (blade pass) intervals, during pump operation. While the two sensors located on the side were used to measure the x and y displacements of the impeller.

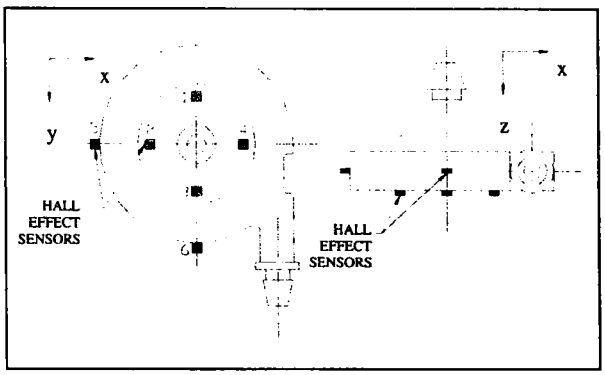

Fig. 3 Location of sensors on the pump

The amplified readings are sent to an analog breakout accessory rack (National Instruments – BNC 2090) and data acquisition board (National Instruments – PC-LPM-16) where the signal is displayed on a computer monitor using a data analysis software (VirtualBench™ V2.1.1). The raw

data was collected by the data acquisition software LabView™ V5.0 (National Instruments, USA)

All six sensors performed measurements simultaneously so that when a blade passed the sensors, all five degrees of freedom of the impeller were measured.

The output signal from the sensors are a DC voltage in the millivolt (mV) range. A simple operational amplifier (Fig. 4) was used for each sensor to amplify the signal.

Four pump operating conditions were investigated. The speed of the pump was adjusted and monitored through the motor commutation controller, while the flow rate was monitored by a

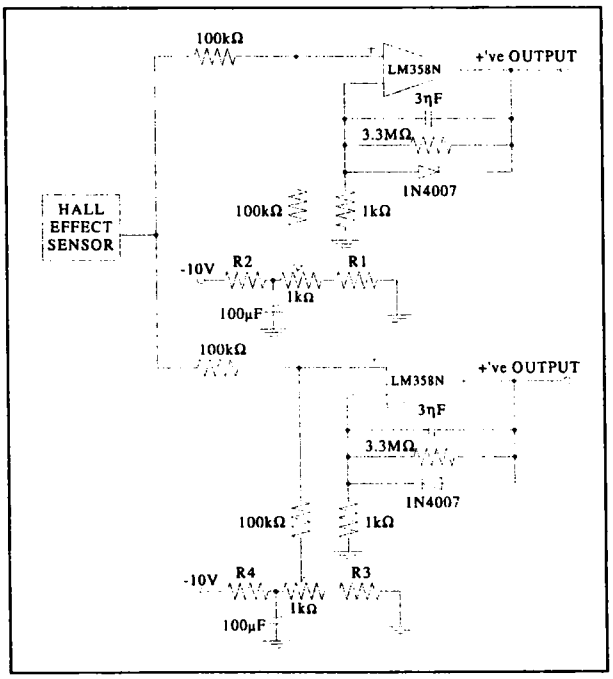

Fig. 4 Circuit diagram of Operational Amplifier

flow probe (#10C277 – Transonic) and a flow meter (T206 – Transonic). The pumping medium used for the experiments was 30% aqueous glycerol. The operating conditions were as follows:

(1) 2000 rev/min @ 2 l/min
(2) 2000 rev/min @ 3 l/min
(3) 2000 rev/min @ 4 l/min
(4) 2000 rev/min @ 5 l/min

A rotating speed of 2000 rev/min was chosen for all conditions due to it being a safe operating speed for final applications. The inflow of the pump was occluded to achieve the flow rates required for each condition.

All sensors have been calibrated individually to ensure the accurate transformation of the output voltage into displacement (μm) values. Calibration involved the use of a computer numerical control (CNC) machine (Benchman XT – Light Machine Corporation 1998) to move the impeller in the x, y and z direction relative to the pump casing. For the axial displacement sensors (1, 2, 3 and 4), the impeller was moved in the z direction at 10 μm intervals from 40 μm to 140 μm. While for the radial sensors, 5 and 6, the impeller was moved in the x and y direction respectively, at 20 μm intervals from –60 μm to 60 μm. All measurements were acquired through LabView at a sampling frequency of 50 kHz. With these results, calibration curves were determined for each sensor. Also, since the magnetic field strength of each of the four blades were not identical, calibration polynomials for each individual blade were also determined.

4. Results and Discussion

Calibration polynomials were determined through the least squares method using Matlab. Orders of polynomials were determined by residual plots as well as calculation of variances. Calibration polynomials for each of the six sensors at each one of the four blades of the impeller were found, resulting in twenty four polynomials.

Output voltages from the sensors for each operating condition were collected through LabView. Samples for 50 impeller revolutions were obtained at a sampling frequency of 38 kHz distributed between the six sensors for all measurements. The corresponding displacement values, in μm, were determined using the calibration polynomials. These values were in turn transformed into displacements in five independent physical coordinates as follows:

$$x = \text{HES } 5 \tag{3}$$

$$y = \text{HES } 6 \tag{4}$$

$$z = \frac{\text{HES } 1 + \text{HES } 3}{2} \tag{5}$$

$$\theta x = \tan^{-1} \frac{\text{HES } 1 - \text{HES } 3}{30000} \tag{6}$$

$$\theta y = \tan^{-1} \frac{\text{HES } 4 - \text{HES } 2}{30000} \tag{7}$$

Where HES 1, HES 2, HES 3, HES 4, HES 5 and HES 6 represents the displacement measurements (in μm) for hall effect sensors 1, 2, 3, 4, 5 and 6 respectively and 30000 represented the distance between opposite sensors.

It must be noted that when the impeller was at the origin of the coordinate system, the displacement in the five independent physical coordinates were 0, 0, 100, 0 and 0 for x, y, z, θx and θy respectively.

The average radial movement (in the x and y direction) for 50 revolutions at each blade pass is shown in Fig. 5.

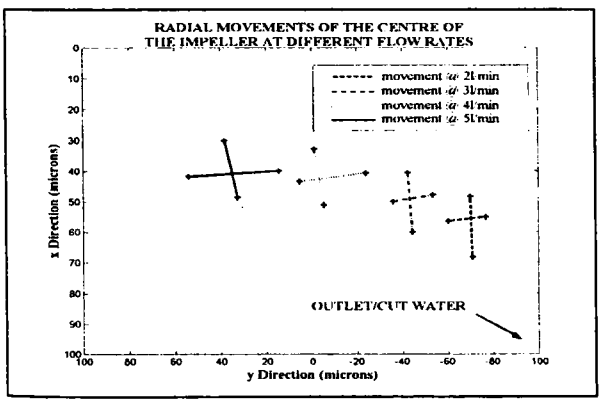

Fig. 5 Radial position of the centre of the impeller for different flow rates

The outlet and cut water of the pump were positioned at the positive x and y direction. From Fig. 6, the range in the x direction increased as the flow also increased. The increase in range represented the decrease in stability of the impeller. This behaviour continued until the maximum efficiency point of the hydrodynamic bearing was reached where the impeller was least stable. Previous investigations have found that the maximum hydraulic efficiency occurred at a flow rate of 6 l/min. At this flow rate, the impeller experienced a minimum resultant radial force due to pressure forces around the volute of the pump being constant. Once the flow rate was changed, the pressure forces became inconsistent around the volute, resulting in an increased resultant force and a more stable impeller. This can be described by the stability parameter[10]:

$$S = \frac{F}{Mc\omega^2} \tag{8}$$

Where the stability parameter (S) represents the stability of the impeller. A decreasing value of S means a decrease in stability for the impeller. S is a function of the resultant radial force (F) of the impeller, mass of the impeller (M), the clearance gap (c) between the impeller and pump cavity and rotational speed (ω) of the impeller. From equation 8, it can be seen that as the radial force approached 0, S also approached 0, resulting in an unstable condition.

Also, Fig. 5 shows the impeller moving towards the outlet/cut water of the pump as the flow was decreasing. This is due to the velocity of the fluid decreasing as it diffused into the outlet, causing the pressure to increase as the velocity decreased. Thus, a low pressure force was experienced after the cut water and a high pressure force at the opposite side of the volute, resulting in a resultant radial force towards the cut water. This phenomenon is typical for centrifugal type pumps (Stepanoff)[11].

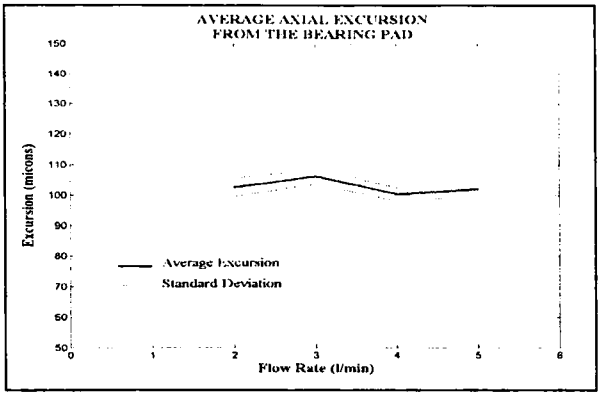

Fig. 6 Average axial excursion at 2000 rev/min

Fig. 6 represents the axial excursion of the impeller. it can be seen that there was almost no change in the axial excursion for increasing flow rates. This coincides with equation 1, which describes the hydrodynamic bearing force, where the bearing force is not a function of the flow rate of the fluid. However, small changes in excursion that were present may be due to the inaccuracies with manually adjusting the commutation of the rotational speed of the impeller from the motor controller.

Results for the angular displacements are as follows:

Table 1 Angular displacement at 2 l/min

Blade Pass	θ_x (radians)	θ_y (radians)
1	0.0007076	-0.0005247
2	0.0005737	-0.0009368
3	0.0010896	-0.0004460
4	0.0004975	-0.0009293

Table 2 Angular displacement at 3 l/min

Blade Pass	θ_x (radians)	θ_y (radians)
1	0.0006481	-0.0000854
2	0.0004874	-0.0004164
3	0.0009783	-0.0000456
4	0.0003268	-0.0003890

Table 3 Angular displacement at 4 l/min

Blade Pass	θ_x (radians)	θ_y (radians)
1	0.0003149	-0.0000272
2	0.0002185	-0.0003611
3	0.0007113	-0.0000796
4	0.0002064	-0.0003522

Table 4 Angular displacement at 5 l/min

Blade Pass	θ_x (radians)	θ_y (radians)
1	-0.0000013	0.0000985
2	0.0000115	0.0000006
3	0.0004394	0.0001193
4	-0.0000833	-0.0000720

From the measured results, the minimum axial displacement for the bottom bearing pad was 96.270605 μm, while the conical surface was 91.5634981 μm. By using the following equation, the angular displacement required for the impeller to touch the pump casing at these axial displacements were found.

$$\theta = \pm \left[\tan^{-1} \left(\frac{2 \times \text{Displacement}}{30000} \right) \right] \qquad (9)$$

θ at the bottom bearing pad was found to be 0.00642 radians, while the conical surface was 0.00610 radians. These θ values represented the maximum angular displacement allowed before the impeller touches the pump casing. It can be clearly seen from tables 1 to 4 that for the experiment carried out, that the angular displacements in both the x and y directions are considerably lower than the calculated angular displacements, indicating that the impeller did not touch the pump casing through angular displacement, even under these worst case operating conditions.

5. Conclusion

The determination of the impeller's displacement within the pump cavity was undertaken experimentally. Hall effect sensors were used for the detection of the impeller within the titanium pump housing. The pump was operated at different flow rates with the impeller rotating at a speed of 2000 rev/min for all conditions.

Results show that under the operating conditions investigated, the impeller was hydrodynamically suspended within the pump cavity.

Maximum and minimum average radial movement of the impeller for each flow rate at a constant impeller speed of 2000 rev/min were obtained. Results were in accordance to centrifugal pump design. Furthermore, the axial excursion of the impeller was also investigated for each flow rate. Again, results were in accordance with pump design.

Overall, the method used to perform the experiment discussed in this paper was successful. Displacement of the impeller in the five independent physical coordinates were determined and found to be acceptable. Results from this experiment can be used for analysis and calculation of the stiffness of the hydrodynamic bearing through computational fluid dynamics.

Acknowledgement

Financial support for this research is provided jointly by the Australian Research Council (Grant No. C8992011), the University of Technology, Sydney and VentrAssist Pty. Ltd. Australia.

References

[1] Kung R T and Hart R M. Design Considerations for Bearingless Rotary Pumps. Artificial Organs, 1997, 21(7): 645-650

[2] Malanoski S B, Belawski H, Horvath D, Smith W A and Golding L R. Stable blood lubricated hydrodynamic journal bearing with magnetic loading. ASAIO Journal, 1998, 44(5): M737-M740

[3] Wampler R, Lancisi D, Indravudh V, Gauthier, R. And Fine R. A sealless centrifugal blood pump with passive magnetic and hydrodynamic bearings, Artificial Organs. 1999, 23(8): 780-784

[4] Mosuzawa T, Kita T, Matsuda K & Okada Y. Magnetically Suspended Rotary Blood pump with radial type combined motor-bearing. Artificial Organs. 2000, 24(6): 468-474

[5] Allaire P, Hilton E, Baloh M, Maslen E, Bearnson G, Noh D, Khanwilkar P & Olsen D. Performance of a continuous flow ventricular assist device: Magnetic bearing design, construction, and testing. Artificial Organs, 1998, 22(6): 475-480

[6] Akamatsu T, Nakazeki T & Itoh H. Centrifugal blood pump with a magnetically suspended impeller. Artificial Organs, 1992, 16(3): 305-308

[7] k Watterson PA, Woodard JC, Ramsden VS & Reizes JA. VentrAssist hydrodynamically suspended, open, centrifugal blood pump. Artificial Organs, 2000, 24(6): 475-477

[8] Cook M & Tansley GD. The dynamic load envelope of the VentrAssist rotary blood pump. In Proceedings of the Second Japan-Australia Cardiovascular Bioengineering Symposium, Sydney, Australia, 2000, 8-9

[9] Massey BS. Mechanics of fluids - 6th Ed. London: Chapman & Hall Publications. 1989.

[10] Akkök M, Ettles CM. The onset of whirl instability in journal bearings of various bore shapes and groove sizes. Transactions of the ASME, 1983, 105(7): 342-352.

[11] Japikse D, Marscher WD, Furst RB. Centrifugal pump design and performance. Vermont, U.S.A.: Concepts ETI, Inc. Publications. 1997